The Chemical and Dynamical Influence of the Anti-Viral Drug Amantadine on the M_2 Proton Channel Transmembrane Domain

Jun Hu,*‡ Riqiang Fu,‡ and Timothy A. Cross*†‡
*Department of Chemistry and Biochemistry, †Institute of Molecular Biophysics, Florida State University; and ‡National High Magnetic Field Laboratory, Tallahassee, Florida

ABSTRACT The M_2 proton channel plays a vital role in the life cycle of the influenza A virus. His^{37}, the key residue in the M_2 transmembrane domain (M_2-TMD), plays a central role in the proton conductance mechanism. The anti-influenza drug, amantadine, inhibits the channel activity through binding to the pore of the M_2 channel. The nuclear spin relaxation data and polarization inversion spin exchange at the magic angle spectra show that both the polypeptide backbone and His^{37} side chain are more constrained in the presence of amantadine. Using ^{15}N cross polarization magic-angle spinning NMR spectroscopy, the protonation of His^{37} of M_2-TMD in lipid bilayers was monitored in the absence and presence of amantadine as a function of pH. Binding amantadine lowers the His^{37} pK_a values by approximately three orders of magnitude compared with the first pK_a of histidine in amantadine-free M_2-TMD. Amantadine's influence on the His^{37} chemical properties suggests a novel mechanism by which amantadine may inhibit proton conductance.

INTRODUCTION

In binding amantadine to the M_2 protein transmembrane domain of influenza A virus several significant effects on the structure, dynamics, and chemical properties of this proton channel are observed (1–5). Here, studies in planar lipid bilayers above the gel-to-liquid-crystalline phase transition and in liposomes below this phase transition temperature were performed using solid-state NMR. While the structural change in the polypeptide backbone as viewed by solid-state NMR has recently been reported (6), here the focus is on the change in dynamics and in the chemical properties of the histidine tetrad formed by His^{37} of this tetrameric protein.

The M_2 protein from influenza A virus is a pH-modulated proton channel that is essential for viral replication (7,8). These viruses enter cells through receptor-mediated endocytosis and are encapsulated by endosomes having a low pH. The M_2 proton channels are activated by low pH and acidify the viral interior leading to the disruption of the interaction between the viral matrix proteins and ribonucleoproteins, a prerequisite process for the release of viral RNA into the cell. In addition to its function in the uncoating process, the M_2 channels also equilibrate the pH between the acidic *trans*-Golgi network and the cytoplasm. Amantadine (1-adamantanamine hydrochloride) is a specific anti-influenza A drug that inhibits viral replication, primarily by binding to the M_2 protein and thereby preventing proton conductance (9–11). Without the acidification of the viral interior, the uncoating process for the influenza A virus fails to occur (12,13). Moreover, the hemagglutinins in the *trans*-Golgi network are forced to adopt a low-pH conformation due to the blocked M_2 channels (14,15).

Although amantadine is effective as a preventative prophylaxis and as a treatment of the influenza A viral infections, its clinical use as an anti-influenza drug is limited due to its central nervous system side effects (16). Rimantadine (α-methyl-1-adamantane-methanamine), an amantadine analog, has been considered a better anti-viral drug because of its enhanced activity and fewer side effects (17,18). However, in the past year, the prevalent Influenza A (H3N2) strain was the S31N mutant that is amantadine-resistant (19). It is generally believed that the rigid amantadine molecule sterically blocks the M_2 transmembrane pore, thereby preventing proton conduction. However, this mechanism remains controversial as it is inconsistent with some of the electrophysiological observations for the M_2 channels (20) and may also be inconsistent with results obtained from amantadine-resistant mutants (4). While the mechanism of amantadine binding to the M_2 channel is unclear, many amantadine analogs have been synthesized to test their antiviral activities (21–23).

The M_2 protein has 96 amino-acid residues with a single 19-residue transmembrane domain (24,25). The functional structure of the M_2 channel is minimally tetrameric (26–28). Electrophysiological studies demonstrate that M_2 protein selectively conducts protons through a variety of membrane systems, such as oocytes of *Xenopus laevis*, mammalian cells, and planar lipid bilayers (29–31). Significant suppression of proton conduction by amantadine or rimantadine in these systems is well documented.

The transmembrane domain of M_2 (M_2-TMD) also forms a proton selective channel in lipid bilayers that is sensitive to amantadine (32). Analytical ultracentrifugation experiments show that amantadine stabilizes the formation of the M_2-TMD tetramer (1). Structural information on M_2-TMD has been obtained by cysteine-mutagenesis (33), molecular dynamics (34), UV resonance Raman spectroscopy (2), Fourier transform infrared spectroscopy (35), solid-state NMR spectroscopy (36–38),

Submitted December 1, 2006, and accepted for publication March 13, 2007.
Address reprint requests to T. A. Cross, Tel.: 850-644-0917; E-mail: cross@magnet.fsu.edu.
Editor: Mark Girvin.

0006-3495/07/07/276/08 $2.00
doi: 10.1529/biophysj.106.102103

and electron spin resonance (39). Uniquely, solid-state NMR has led to a high-resolution backbone structure of the monomer while in a tetramer configuration (PDB ID: 1MP6, (36)). The addition of a precise distance restraint between helices has resulted in a structure of the tetrameric transmembrane domain (PDB ID: 1NYJ; (38)). Interestingly other spectroscopic data suggests somewhat different tilt angles for the helices depending on the membrane mimetic environment (39). The M_2-TMD structure built on the basis of solid-state NMR orientational and distance restraints indicates a channel pore lined by polar residues (Ser^{31}, His^{37}, and Trp^{41}) that can accommodate an amantadine molecule (38). Nevertheless, spectroscopic evidence from fluorescence (1) and circular dichroism (3) indicates that some structural rearrangement takes place upon amantadine binding. The M_2-TMD/amantadine model proposed by Gandhi et al. (40) reflects some insights for this structural alteration and suggests a potential hydrogen-bonding interaction between the nonprotonated His^{37} $N^{\delta1}$ and the amantadine amino group. Recently, the backbone structure of the amantadine-bound state has been determined (PDB ID: 2H95; (6)) showing a kinked helical structure, but the position of amantadine within the structure was not defined.

Here, by using ^{15}N cross-polarization magic-angle spinning (CPMAS) NMR spectroscopy, we titrated the M_2-TMD histidine in the presence and absence of amantadine as a function of pH. The effect of amantadine binding on the His^{37} side-chain motion was studied by comparing the cross polarization efficiency for the His^{37} $^{15}N^{\delta1}$ signal with and without amantadine. The conformational and dynamic changes in the M_2-TMD backbone upon amantadine binding were also monitored by polarization inversion spin exchange at the magic angle (PISEMA) experiments (41,42).

MATERIALS AND METHODS

Peptide synthesis and sample preparation

$^{15}N^{\delta1}$ histidine and $^{15}N^{\varepsilon2}$ histidine were purchased from Cambridge Isotope Laboratories (Cambridge, MA) and chemically protected by trityl and 9-fluorenylmethoxycarbonyl (Fmoc) groups following literature procedures (43,44). The total yield of 9-fluorenylmethoxycarbonyl -His-(trityl)-OH was 73–81%. The M_2-TMD peptide, NH_2-Ser^{22}-Ser-Asp-Pro-Leu-Val-Val-Ala-Ala^{30}-Ser-Ile-Ile-Gly-Ile-Leu-($^{15}N^{\delta1}$ or $^{15}N^{\varepsilon2}$)His^{37}-Leu-Ile-Leu^{40}-Trp-Ile-Leu-Asp-Arg-Leu^{46}-COOH was chemically synthesized by solid-phase synthesis on an Applied Biosystems (Foster City, CA) model No. 430A synthesizer. The peptides were purified and characterized as described previously (37).

^{15}N His^{37} labeled M_2-TM domain was incorporated into liposomes through the assistance of a detergent, 1-O-octyl-β-D-glucopyranoside (OG) (45). First 10 mg M_2-TMD peptide, 40 mg 1,2-dimyristoyl-*sn*-3-phosphocholine (DMPC), 10 mg 1,2-dimyristoyl-*sn*-glucero-3-[phospho-*rac*-(1-glycerol)] (DMPG), and 320 mg OG were codissolved in 20 ml 2,2,2-trifluoroethanol (TFE) and chloroform (v/v: 4/1). An OG/lipid ratio of 15:1 allows for the preparation of a highly homogeneous sample of vesicles after OG is dialyzed out later in this procedure (46). The organic solvent was evaporated from a rotary flask and then the mixture was placed under high vacuum for at least 6 h to remove residual organic solvent. Fifteen milliliters of 10 mM citrate-borate-phosphate (CBP) buffer of a specific pH with 1 mM ethylenediaminetetraacetic acid was added to the dried mixture and a clear solution was prepared after the flask was shaken in a bath for ~20 min at 37°C (above the gel-to-liquid-crystalline phase transition temperature of DMPC (~23°C) (47). This solution was then transferred into a dialysis bag with a 3 kDa cutoff and dialyzed at 4°C against the buffer, which was changed at least five times in five days to ensure virtually complete removal of the detergent. For an M_2-TMD sample with 10 mM amantadine, 46.9 mg (250 μmol) amantadine hydrochloride (Thermo Fisher Scientific, Waltham, MA) in 5 ml CBP buffer was added to an M_2-TMD loaded vesicle suspension (20 ml). The suspension was incubated at room temperature overnight and pelleted in 2.5 h by ultracentrifugation at 196,000 *g*. The pH value of the pellet was implied from a measurement of the supernatant. Finally, the M_2-TMD in DMPC/DMPG liposomes with or without amantadine was packed into a 7 mm Bruker (Madison, WI) zirconia magic-angle rotor with a sealing cap ready for CPMAS NMR experiments.

Oriented samples of the ^{15}N-(L26, L36, L38, L40, L43) and $^{15}N^{\varepsilon2}$ His labeled peptide in hydrated DMPC bilayers were prepared by first codissolving M_2-TMD (20 mg) and DMPC (75 mg) in 10 ml TFE. TFE was removed by rotary evaporation and dried further under high vacuum. Fifteen milliliters of 2 mM CBP buffer (~37°C, pH 8.8) with 1 mM ethylenediaminetetraacetic acid was added to the dried mixture and shaken at 37°C. This lipid suspension was bath-sonicated for 10 min intermittently. The sonicated suspension was loaded into a 1 kDa cutoff dialysis bag. The dialysis bag was placed in 1 L of 2mM CBP buffer overnight to adjust the pH of the M_2-TMD/DMPC liposomes. For the samples with amantadine, the outside buffer contained 10 mM amantadine. The liposomes were passed through a 2-μm filter and pelleted by ultracentrifugation at 196,000 *g*. As above, the pH of the supernatant was measured with an accuracy of $\pm$0.05. The pellet was agitated at 37°C for 1 h until fluid. This viscous fluid was spread onto 50 glass slides (5.7 mm $\times$ 12.0 mm) (Marienfeld Glassware, Bad Margentheim, Germany) and dried in a constant humidity (70–75% relative humidity) chamber using an N_2 atmosphere. The dehydrated slides were rehydrated with 1.5 μl, 2 mM CBP buffer per slide followed by stacking the slides into a glass tube. The sample was incubated at 43°C for 24 h in 96% humidity (saturated K_2SO_4) chamber. Finally, the glass tube was sealed at both ends with epoxy and two glass caps.

Solid-state NMR experiments

All CPMAS NMR experiments were conducted on a Bruker DMX-300 NMR spectrometer at 277 K using a spinning rate of 3 kHz. Two milliseconds cross-polarization contact time and 5 s recycle delay were used throughout the variable-pH NMR experiments. One-hundred Hertz exponential line broadening was applied to the free induction decay before Fourier transform. Static ^{31}P NMR experiments on oriented samples at 303 K were also performed using the Bruker DMX-300 NMR spectrometer with an NHMFL $^{31}P/^{1}H$ double resonance probe. The two-dimensional PISEMA experiments were performed at 303 K on a 400 MHz spectrometer using an NHMFL $^{15}N/^{1}H$ double resonance probe. Typically, a 6 s delay was applied before the ^{1}H 90° pulse (52.1 kHz field). This RF field was also applied during the ^{1}H-^{15}N cross polarization (800 μs) and ^{1}H continuous wave decoupling, while an RF field of 63.7 kHz was used during the Lee-Goldberg spin exchange at the magic angle. Proton carrier frequencies were carefully adjusted to minimize the offset effect (48,49). Thirty-two t_1 increments with 512 or 1024 transients were recorded for the two-dimensional PISEMA spectra. ^{15}N chemical shift of a saturated $^{15}NH_4NO_3$ was defined as 0 ppm for all ^{15}N spectra.

The ^{1}H spin-lattice relaxation time in the rotating frame ($T_{1\rho}^{H}$) was measured using a standard pulse sequence described previously (50,51). In short, after a 90° pulse on the ^{1}H channel, the ^{1}H magnetization was spin-locked for a period of time τ_{SL} before making CP contact with the ^{15}N spins. With a fixed CP contact time (2 ms), the polarized ^{15}N signals detected with ^{1}H decoupling monitored the ^{1}H magnetization in the spin-lock field as a function of τ_{SL}, thus allowing one to measure $T_{1\rho}^{H}$ indirectly. For variable-contact

CP experiments, CP occurs right after the first 90° ^{1}H pulse and the contact time was varied from 100 μs to 10 ms (50).

RESULTS AND DISCUSSION

Amantadine binding effect on M_2-TMD resonances

Chemical structures and the chemical shift resonances of histidine side chains in M_2-TMD depend upon the local environment. In addition, neutral histidines may also undergo tautomerization. Fig. 1 illustrates the resonance assignment of histidines for the different chemical states in the M_2-TMD channel (52). Generally, $^{15}N^{\varepsilon2/\delta1}$-^{1}H of positively charged histidines contributes to signals in the range of 153–156 ppm (53), while the neutral histidine side chains give rise to chemical shifts between 144 and 147 ppm. Neutral $^{15}N^{\delta1}$-^{1}H loses a proton due to tautomerization, resulting in $^{15}N^{\delta1}$ signals resonating at 230 ppm. $HisH^{+}$-His hydrogen-bonding shifts $^{15}N^{\varepsilon2/\delta1}$-^{1}H to a lower field, while the nonprotonated nitrogen shifts to a higher field (60). For M_2-TMD in the absence of amantadine, the protonated nitrogen was observed between 162 and 167 ppm (52).

Fig. 2 *A* displays the CPMAS NMR spectra of $^{15}N^{\varepsilon2}$ labeled His^{37} M_2-TMD with and without amantadine at pH 8.8. The ^{15}N chemical shifts of 144 ppm indicate that histidines are neutral in both cases at this pH. The striking difference in these spectra is the improvement in linewidth upon binding amantadine, suggesting that the amplitude of low frequency motions has been dramatically reduced or that conformational heterogeneity has been greatly reduced upon amantadine binding. Shown in Fig. 2 *B* is PISEMA data from the ^{15}N-Leucine labeled M_2-TMD prepared in an analogous fashion to the ^{15}N His^{37} samples. Once again, a dramatic improvement in linewidth is observed upon binding amantadine. Consequently, if there is a reduction in low frequency motion it pertains to both the histidine side chain and the backbone throughout the TM helix. Furthermore, since the

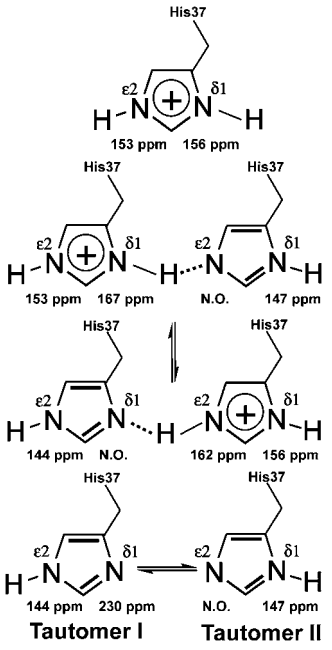

FIGURE 1 Chemical shift assignments associated with the chemical states of histidines in M_2-TMD. In the presence of amantadine, His -$HisH^{+}$ dimerization does not occur. (*N.O.*, not observed.)

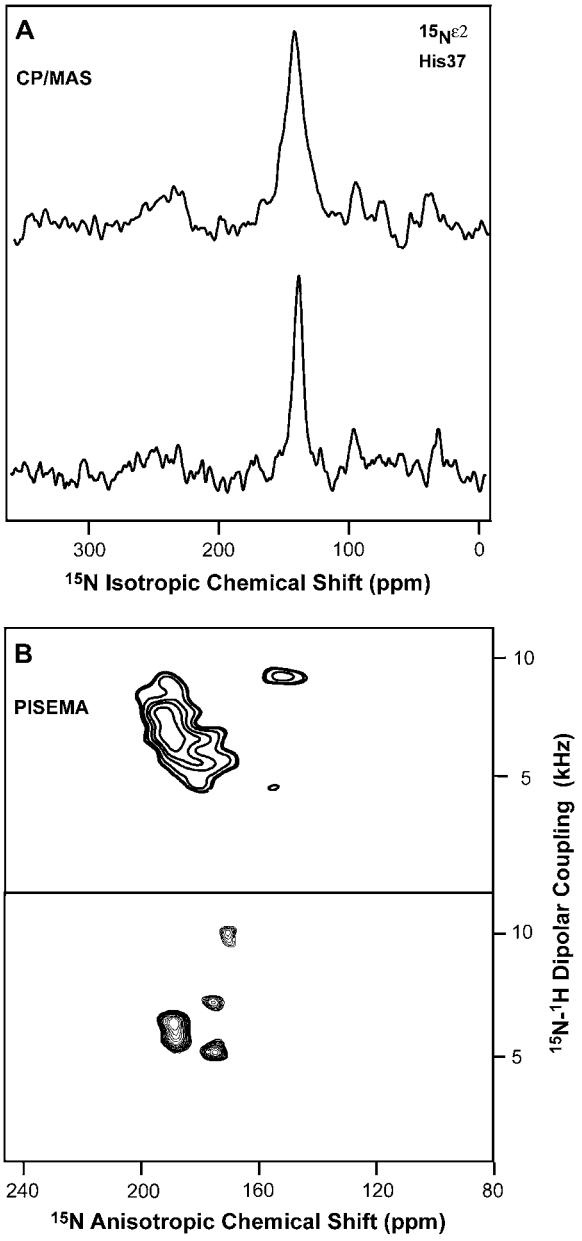

FIGURE 2 ^{15}N solid-state NMR spectra of M_2-TMD in lipid bilayer environments with (*bottom*) and without (*top*) amantadine bound. (*A*) CPMAS NMR spectra of His^{37} ($^{15}N^{\delta1}$) M_2-TMD in DMPC/DMPG (4:1 molar ratio) at pH 8.8. Spectra were obtained at 277 K with a spinning rate of 3 kHz. (*B*) PISEMA spectra of five-site ^{15}N leucine labeled M_2-TMD at pH 9.0 in DMPC bilayers at 298 K.

PISEMA resonances directly and sensitively reflect the orientation of these backbone sites with respect to the laboratory frame, the well-resolved resonances in the M_2-TMD/amantadine spectrum define a unique structure with little orientational mosaic spread. Either local (peptide plane) or global (helix) disorder would broaden the resonances in the PISEMA spectrum. Such a situation is observed when amantadine is absent, but not in its presence. In addition, the PISEMA spectrum of $^{15}N^{\varepsilon 2}$-His^{37} M_2-TMD in the presence of amantadine at pH 9 shows a well-defined splitting (Fig. 3) consistent with a unique conformation having little disorder (54). As indicated from thermal stability studies of M_2-TMD mutants (5), the dynamics or conformational heterogeneity in the absence of amantadine when the channel is functional appears to require structural flexibility to be sensitive to the chemical stimulus (e.g., H^+).

Slow dynamics of the His^{37} side chain

In the CPMAS experiments, it is not possible to quantitatively compare the intensities of the protonated and nonprotonated ^{15}N resonance intensities directly. For the case where $T_{1\rho}^H$ is approximately equal to the CP buildup time T_{NH}, Fu and co-workers developed a Lee-Goldburg frequency-modulated CP approach to improve the $T_{1\rho}^H$ and CP buildup rate (50). Under long CP contact conditions, a relatively accurate estimate of the ratio between nonprotonated and protonated histidine resonances is achieved by integrating the signals in the Lee-Goldburg frequency-modulated CP spectrum. For membrane protein samples in hydrated lipid bilayers, T_{NH} is often similar to or even longer than $T_{1\rho}^H$. In this case, it is inappropriate to apply the above methods to define the relative amount of each component in the CPMAS NMR spectrum and we have resorted here to analyzing the cross polarization kinetics followed by the development of a correction factor to calculate the relative number of protonated and nonprotonated sites. In addition to the measurements of

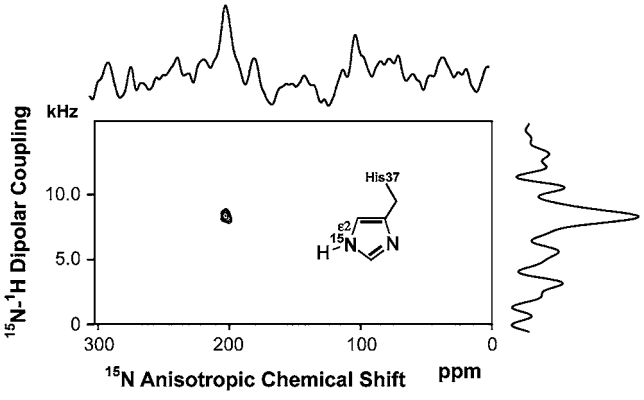

FIGURE 3 ^{15}N PISEMA spectra of $^{15}N^{\varepsilon 2}$ His^{37} labeled M_2-TMD in aligned DMPC planar bilayers with amantadine bound at pH 9.0. The PISEMA spectra were acquired on a 400 MHz spectrometer at 298 K.

$T_{1\rho}^H$ and T_{NH}, the intensities of the spinning side bands for the nonprotonated state must also be included (50).

The mobility of the His^{37} side chain can be assessed by measuring the relaxation parameters controlling the ^{15}N CP process. Here, we make the reasonable assumption that T_{NH} is much shorter than the ^{15}N spin-lattice relaxation time in the rotating frame ($T_{1\rho}^N$, (55)). Then the signal intensity of a given species, $M_{(\tau_{CP})}$, can be characterized by the equation (56)

$$M_{(\tau_{CP})} = M_0\left(1-\frac{T_{NH}}{T_{1\rho}^H}\right)^{-1}\left[\exp\left(-\frac{\tau_{CP}}{T_{1\rho}^H}\right)-\exp\left(-\frac{\tau_{CP}}{T_{NH}}\right)\right], \quad (1)$$

where τ_{CP} is the CP contact time and M_0 is a constant that is proportional to the number of spins. Using a standard CP experiment (51), $T_{1\rho}^H$ can be measured experimentally by fitting the signal intensities as a function of spin-lock time before CP τ_{SL} with

$$M_{(\tau_{SL})} = M_0\exp\left(-\frac{\tau_{SL}}{T_{1\rho}^H}\right). \quad (2)$$

Using the $^{15}N^{\delta 1}$-His^{37} M_2-TMD sample at pH 8.8, data for both the 147 ppm and 230 ppm resonances were collected simultaneously. The values of $T_{1\rho}^H$, M_0, and T_{NH} in the absence and presence of amantadine are listed in Table 1.

The inverse of the CP buildup time of the dilute spin ^{15}N signal cross-polarized from the abundant spin ^{1}H, $1/T_{NH}$, more often called the CP rate constant, is predominantly controlled by the NH dipolar coupling. Roughly, the CP rate is proportional to the square of the dipolar coupling between ^{1}H and ^{15}N (57,58). This explains why the signal buildup for the protonated $^{15}N^{\delta 1}$ (147 ppm) resonance is approximately two orders-of-magnitude faster than for the nonprotonated resonance (230 ppm). Consequently, the observed intensities for protonated and nonprotonated sites at a single cross-polarization time cannot be compared directly without taking the cross-polarization kinetics into account.

Molecular motions can average and hence reduce dipolar interactions and therefore T_{NH} can provide a qualitative description of the motional difference in the presence and absence of amantadine. Here we assume that the magic angle spinning rate does not affect the T_{NH} values (59) and that the Hartmann-Hahn condition was well matched. In the presence of amantadine, T_{NH} is approximately half that in its absence. In other words, the ^{15}N-^{1}H dipolar interaction in the absence of amantadine is 22% smaller due to the motional averaging in the His^{37} side chain. For amantadine-bound M_2-TMD, both the backbone (Fig. 2 *B*) and side-chain (Fig. 3) PISEMA data suggest less conformational heterogeneity and/or reduced motional amplitude. Coupled with the T_{NH} results, it is clear that the amantadine-bound state is more rigid and conformationally more homogeneous. In addition, the PISEMA data for amantadine-bound M_2-TMD has been used to characterize an altered backbone structure involving a kinked α-helical structure (6).

TABLE 1 Summary of NMR relaxation parameters and relative population of $^{15}N^{\delta1}$ 230 ppm and 147 ppm signals

	$T_{1\rho}^{H}$ (ms)*		T_{NH} (μs)*		M_0		Relative amount†	
Peak position (ppm)	With amantadine	No amantadine‡	With amantadine	No amantadine‡	With amantadine	No amantadine‡	With amantadine	No amantadine‡
230 (≥N)	4.2 ± 0.9	5.2 ± 1.6	6900 ± 590	11400 ± 420	9.9 ± 0.3	286 ± 9	3.3	3.5
147 (>N-H)	4.8 ± 1.6	5.1 ± 0.9	65 ± 30	170 ± 30	3.0 ± 0.3	81 ± 3	1	1

*The errors are obtained from the curve fitting to Eqs. 1 and 2.
†The relative amount is calculated from the ratio of M_0 between different species.
‡The amantadine-free data were adopted from Hu (54).

His^{37} tautomerization

On the basis of the values of M_0 for the 147 and 230 ppm resonances, the nonprotonated $\delta1$ tautomer was found to be at least three times more favorable than the protonated $\delta1$ tautomer (Table 1). Amantadine does not appear to change the population of the two tautomers. In solution, free histidine favors the nonprotonated $\delta1$ tautomer with an ~4:1 ratio (60). It is intriguing that the neutral histidines in the M_2-TMD channel behave similarly as they do in the bulk solution. This ratio suggests that one out of four histidines is in the $\delta1$-protonated tautomeric state and hence is unlikely to be adjacent to another $\delta1$-protonated His^{37} residue.

Even without charged residues, the presence of both tautomeric forms breaks the fourfold symmetry of the structure. The observation of distinct nonprotonated (230 ppm) and protonated (147 ppm) sites clearly demonstrates that the His^{37} residues undergo side-chain tautomerization at a rate slower than 2.5 kHz based on the separation of these two resonances in Hz for a sample in a 7 Tesla magnet (30 Hz/ppm × 83 ppm). At the same time, one might expect structural differences based on the tautomer heterogeneity that would be observed in the PISEMA spectra. We can expect a protonated $^{15}N^{\varepsilon2}$ imidazole to be located in each of the three positions in the tetrad with a nonprotonated residue in the other site. Each of these imidazoles has a different local environment based on the protonation of the imidazoles on either side and each configuration could result in a different orientation for the $^{15}N^{\varepsilon2}$ imidazole. The observation of a unique ^{15}N-^{1}H dipolar coupling and ^{15}N chemical shift for both the $^{15}N^{\varepsilon2}$ sites (Fig. 3) and the polypeptide backbone (Fig. 2 *B*) suggest that the structural difference causes <2 kHz change in the dipolar splitting; otherwise, multiple splittings would be observed. Such a small change in dipolar splitting translates to very small changes in either the backbone amide planes or the imidazole ring orientations.

Low proton affinity of His^{37} with amantadine

Fig. 4 shows the pH titration for the $\delta1$ site in the presence and absence of amantadine. Resonances at 230 and 147 ppm arise from the nonprotonated and protonated (neutral) $^{15}N^{\delta1}$ sites, respectively (54). In addition to the neutral tautomeric states, two additional resonances are observed. The resonances at 156 ppm represent the biprotonated charged state and the broad resonance at 167 ppm (only in the absence of amantadine) reflects the formation of the His-HisH$^+$ dimer (52,61). In the absence of amantadine the observed resonance intensities (corrected for cross-polarization kinetics and spinning side-band intensities) have been interpreted to yield a set of pK_a values for this histidine tetrad: 8.2, 8.2, 6.3, and <5.0 (Fig. 5). As discussed previously (52) this titration results in a couple of unique conclusions. The first two histidines to titrate appear to titrate with cooperative proton binding and at very high pH compared to the normal pK_a of histidine. Secondly, the binding of these protons appear to form His-HisH$^+$ dimers that distribute the charge through the formation of low-barrier hydrogen bonds.

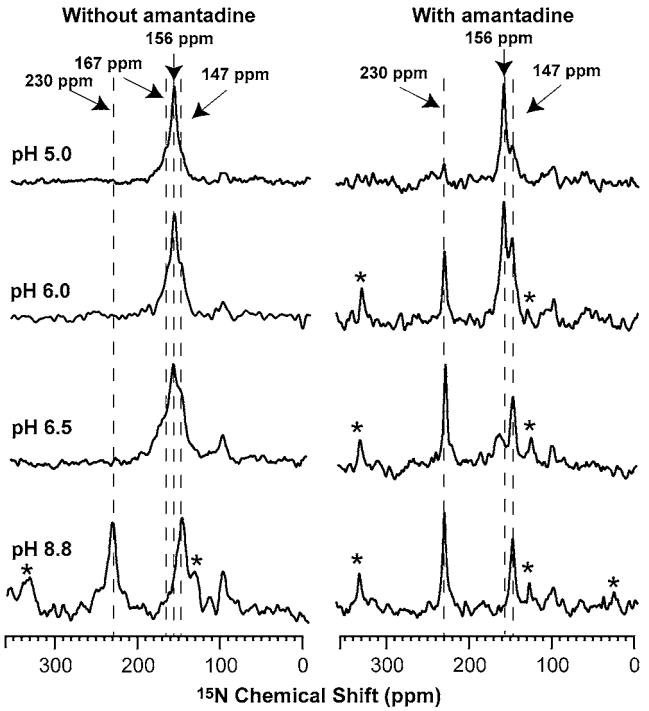

FIGURE 4 CPMAS NMR spectra of His^{37} ($^{15}N^{\delta1}$) M_2-TMD with and without amantadine at different pH values. Spectra were obtained on a Bruker DMX-300 NMR spectrometer at 277 K with a spinning rate of 3 kHz. Signals at ~100 ppm are from the natural abundance amides from the M_2-TMD backbone. Spinning side bands are marked with asterisks.

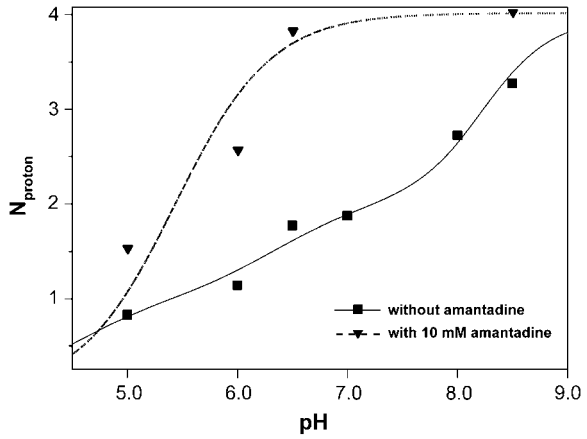

FIGURE 5 Curves for N_{proton} versus pH in the presence (*dashed line*) and absence (*solid line*) of 10 mM amantadine. N_{proton} is the number of released protons from the His^{37} tetrad at a given pH value. At each pH value, N_{proton} was calculated on the basis of the ratio of M_0 for different histidine species (54). The N_{proton} versus pH data in the presence of amantadine were fitted assuming that there is a single kind of titratable histidine in the channel, while for the amantadine-free M_2-TMD multiple titration states must be considered and the fitting curve was adopted from Hu et al. (52) for the purpose of comparison. Both fitting curves were generated using the nonlinear regression fitting program in Origin 6 (Microcal Software, Northampton, MA).

In the presence of amantadine, there are two striking changes in the pH titration. First, the nonprotonated $\delta 1$ resonance, indicative of the uncharged monomeric state, is present even at pH 5, while in the absence of amantadine this resonance disappeared between pH 7.0 and 8.0. Consequently, the first pK_a values for this histidine tetrad have shifted to much lower pH values in the presence of amantadine. Secondly, there is little or no evidence for a resonance at 167 ppm, suggesting that the His-$HisH^+$ dimer does not form in the presence of amantadine. As shown in Fig. 5, the pK_a values appear to be in the vicinity of 5.4. The protonation at this pH does not appear to be associated with the dissociation of amantadine from M_2-TMD, based on the narrow linewidths observed even at very low pH in the presence of amantadine. Neither is it very reasonable to propose uniform pK_a values for each of the four His^{37} residues, unless the tetrameric structure is not stable below this pH. The tetramerization studies for M_2-TMD suggest that the tetramer is not very stable below pH 6 in micelles (1); however, it is anticipated to be much more stable in lipid bilayers, as suggested by the conductance studies of M_2-TMD (32,52). In addition, it has been shown that binding amantadine to M_2-TMD (1) stabilizes the tetrameric complex. Consequently, we do not anticipate that the tetramer is dissociating at this pH. However, it is likely that there is a structural change that is permitting multiple protonations of the His^{37} residues at this low pH. Unfortunately, it is difficult to obtain structural data at this pH due to conformational heterogeneity (54).

The lack of His-$HisH^+$ dimer suggests that water is in an appropriate orientation to access the imidazole nitrogens and to compete for these hydrogen-bonding sites, thereby preventing the formation of low-barrier His-$HisH^+$ hydrogen bonds. This appears to be in conflict with the Trp^{41} fluorescence emission results reported by Salom et al. (1), in which they suggest that, upon binding amantadine, the environment for Trp^{41} becomes more hydrophobic. However, other explanations for the failure to form His-$HisH^+$ dimers are also possible; for instance, the cooperativity in proton binding in the absence of amantadine suggests that a structural change is induced by the formation of the first His-$HisH^+$ dimer and that the resultant tense state is relieved when a second proton is bound, forming a second and symmetric His-$HisH^+$ dimer. The observed titration in the presence of amantadine may then be consistent with the formation of individual biprotonated histidines in the M_2-TMD.

The influence of amantadine on the chemical properties of this histidine tetrad observed here suggests the possibility of a novel mechanism for how amantadine may inhibit proton conductance. It has long been assumed that amantadine sterically blocks the pore formed by the M_2 protein four-helix bundle. However, Arkin and co-workers (4), in studying amantadine resistant mutants by surface plasmon resonance, has observed that a subset of these mutants still bind amantadine and yet proton conductance is not blocked. While it is possible to make an argument on steric grounds to explain this result, it is also possible to speculate that the influence of amantadine on the chemical properties of the histidine tetrad could be modified in these mutants and hence form a distinct functional mechanism.

In conclusion, the structure of the transmembrane domain of M_2 at high pH and in the absence of amantadine is more dynamic and structurally heterogeneous compared with the structure when amantadine is bound. It is likely that the dynamics and structural plasticity are essential for the functional complexity of channel opening, gating, and proton conduction, both for the isolated transmembrane domain and for the full-length protein. There is growing evidence in the literature that there is a large number of membrane proteins for which the transmembrane domain and water-soluble domain, at least in part, function separately. For instance, the CorA Mg^{2+} transporter structure was recently solved by crystallizing the water-soluble domain and then using that structure to solve the full-length protein structure (62). Many properties of the M_2 transmembrane domain and the full-length protein appear to be, at least, qualitatively the same, such as tetramerization, proton conductance, and amantadine binding. Here, amantadine appears to interfere with the unique chemistry of the histidine tetrad in the transmembrane domain; we would anticipate the same in the full-length protein. Not only are the pK_a values drastically altered, but the formation of low-barrier hydrogen bonds appears to be impossible in the presence of amantadine—suggesting that the mechanism by which amantadine prevents proton conductance may not be steric hindrance, but instead a mechanism that interferes with the histidine facilitation.

The authors are grateful to the staff of National High Magnetic Field Laboratory NMR facility (A. Blue) and the staff of Bioanalytical Synthesis and Service Laboratory (H. Hendricks and U. Goli) for their expertise, assistance, and maintenance of the instruments essential for this work.

This work was supported by the National Science Foundation (grant No. MCB02-35774) and the National Institutes of Health (grant No. AI 23007). The experiments were largely performed at the National High Magnetic Field Laboratory, supported by Cooperative Agreement No. DMR-0084173 and the State of Florida.

REFERENCES

1. Salom, D., B. R. Hill, J. D. Lear, and W. F. DeGrado. 2000. pH-dependent tetramerization and amantadine binding of the transmembrane helix of M_2 from the influenza A virus. *Biochemistry.* 39:14160–14170.
2. Okada, A., T. Miura, and H. Takeuchi. 2001. Protonation of histidine and histidine-tryptophan interaction in the activation of the M_2 ion channel from influenza a virus. *Biochemistry.* 40:6053–6060.
3. Duff, K. C., S. M. Kelly, N. C. Price, and J. P. Bradshaw. 1992. The secondary structure of influenza A M_2 transmembrane domain. A circular dichroism study. *FEBS Lett.* 311:256–258.
4. Astrahan, P., I. Kass, M. A. Cooper, and I. T. Arkin. 2004. A novel method of resistance for influenza against a channel-blocking antiviral drug. *Proteins.* 55:251–257.
5. Stouffer, A. L., V. Nanda, J. D. Lear, and W. F. DeGrado. 2005. Sequence determinants of a transmembrane proton channel: an inverse relationship between stability and function. *J. Mol. Biol.* 347:169–179.
6. Hu, J., T. Asbury, S. Achuthan, C. Li, R. Bertram, J. Quine, R. Fu, and T. A. Cross. 2006. Backbone structure of the amantadine-blocked transmembrane domain M_2 proton channel from influenza A virus. *Biophys. J.* In press.
7. Lamb, R. A., and R. M. Krug. 1996. Fields Virology. B. N. Fields, D. M. Knipe, and P. M. Howley, editors. Lippincott-Raven Publishers, Philadelphia, PA.
8. Lamb, R. A., L. J. Holsinger, and L. H. Pinto. 1994. The Influenza A Virus M_2 Ion Channel Protein and its Role in the Influenza Virus Life Cycle. Cold Spring Harbor Laboratory Press, Cold Spring Harbor, New York.
9. Wang, C., K. Takeuchi, L. H. Pinto, and R. A. Lamb. 1993. Ion channel activity of influenza A virus M_2 protein: characterization of the amantadine block. *J. Virol.* 67:5585–5594.
10. Hay, A. J. 1992. The action of adamantanamines against influenza A viruses: inhibition of the M_2 ion channel protein. *Semin. Virol.* 3:21–30.
11. Hay, A. J., A. J. Wolstenholme, J. J. Skehel, and M. H. Smith. 1985. The molecular basis of the specific anti-influenza action of amantadine. *EMBO J.* 4:3021–3024.
12. Kato, N., and H. J. Eggers. 1969. Inhibition of uncoating of fowl plague virus by l-adamantanamine hydrochloride. *Virology.* 37:632–641.
13. Skehel, J. J., A. J. Hay, and J. A. Armstrong. 1978. On the mechanism of inhibition of influenza virus replication by amantadine hydrochloride. *J. Gen. Virol.* 38:97–110.
14. Ciampor, F., P. M. Bayley, M. V. Nermut, E. M. Hirst, R. J. Sugrue, and A. J. Hay. 1992. Evidence that the amantadine-induced, M_2-mediated conversion of influenza A virus hemagglutinin to the low pH conformation occurs in an acidic *trans* Golgi compartment. *Virology.* 188:14–24.
15. Grambas, S., M. S. Bennett, and A. J. Hay. 1992. Influence of amantadine resistance mutations on the pH regulatory function of the M_2 protein of influenza A viruses. *Virology.* 191:541–549.
16. Skehel, J. J. 1992. Influenza virus. Amantadine blocks the channel. *Nature.* 358:110–111.
17. Dolin, R., R. C. Reichman, H. P. Madore, R. Maynard, P. N. Linton, and J. Webber-Jones. 1982. A controlled trial of amantadine and rimantadine in the prophylaxis of influenza A infection. *N. Engl. J. Med.* 307:580–584.
18. Tsunasawa, S., T. Masaki, M. Hirose, M. Soejima, and F. Sakiyama. 1989. The primary structure and structural characteristics of *Achromobacter lyticus* protease I, a lysine-specific serine protease. *J. Biol. Chem.* 264:3832–3839.
19. Bright, R. A., D. Shay, J. Bresee, A. Klimov, N. Cox, and J. Ortiz. 2006. High levels of adamantane resistance among influenza A (H3N2) viruses and interim guidelines for use of antiviral agents. United States, 2005–2006 influenza season. *MMWR Morb. Mortal. Wkly. Rep.* 55: 44–46.
20. Pinto, L. H., and R. A. Lamb. 1995. Understanding the mechanism of action of the anti-influenza virus drug amantadine. *Trends Microbiol.* 3:271.
21. Aldrich, P. E., E. C. Hermann, W. E. Meier, M. Paulshock, W. W. Prichard, J. A. Snyder, and J. C. Watts. 1971. Antiviral agents. 2. Structure-activity relationships of compounds related to 1-adamantanamine. *J. Med. Chem.* 14:535–543.
22. Kolocouris, N., A. Kolocouris, G. B. Foscolos, G. Fytas, J. Neyts, E. Padalko, J. Balzarini, R. Snoeck, G. Andrei, and E. De Clercq. 1996. Synthesis and antiviral activity evaluation of some new aminoadamantane derivatives. 2. *J. Med. Chem.* 39:3307–3318.
23. Scholtissek, C., G. Quack, H. D. Klenk, and R. G. Webster. 1998. How to overcome resistance of influenza A viruses against adamantane derivatives. *Antiviral Res.* 37:83–95.
24. Lamb, R. A., and P. W. Choppin. 1981. Identification of a second protein (M_2) encoded by RNA segment 7 of influenza virus. *Virology.* 112:729–737.
25. Lamb, R. A., S. L. Zebedee, and C. D. Richardson. 1985. Influenza virus M_2 protein is an integral membrane protein expressed on the infected-cell surface. *Cell.* 40:627–633.
26. Holsinger, L. J., and R. A. Lamb. 1991. Influenza virus M_2 integral membrane protein is a homotetramer stabilized by formation of disulfide bonds. *Virology.* 183:32–43.
27. Panayotov, P. P., and R. W. Schlesinger. 1992. Oligomeric organization and strain-specific proteolytic modification of the virion M_2 protein of influenza A H1N1 viruses. *Virology.* 186:352–355.
28. Sugrue, R. J., and A. J. Hay. 1991. Structural characteristics of the M_2 protein of influenza A viruses: evidence that it forms a tetrameric channel. *Virology.* 180:617–624.
29. Chizhmakov, I. V., F. M. Geraghty, D. C. Ogden, A. Hayhurst, M. Antoniou, and A. J. Hay. 1996. Selective proton permeability and pH regulation of the influenza virus M_2 channel expressed in mouse erythroleukemia cells. *J. Physiol.* 494:329–336.
30. Vijayvergiya, V., R. Wilson, A. Chorak, P. F. Gao, T. A. Cross, and D. D. Busath. 2004. Proton conductance of influenza virus M_2 protein in planar lipid bilayers. *Biophys. J.* 87:1697–1704.
31. Mould, J. A., H. C. Li, C. S. Dudlak, J. D. Lear, A. Pekosz, R. A. Lamb, and L. H. Pinto. 2000. Mechanism for proton conduction of the M_2 ion channel of influenza A virus. *J. Biol. Chem.* 275:8592–8599.
32. Duff, K. C., and R. H. Ashley. 1992. The transmembrane domain of influenza A M_2 protein forms amantadine-sensitive proton channels in planar lipid bilayers. *Virology.* 190:485–489.
33. Pinto, L. H., G. R. Dieckmann, C. S. Gandhi, C. G. Papworth, J. Braman, M. A. Shaughnessy, J. D. Lear, R. A. Lamb, and W. F. DeGrado. 1997. A functionally defined model for the M_2 proton channel of influenza A virus suggests a mechanism for its ion selectivity. *Proc. Natl. Acad. Sci. USA.* 94:11301–11306.
34. Sansom, M. S., I. D. Kerr, G. R. Smith, and H. S. Son. 1997. The influenza A virus M_2 channel: a molecular modeling and simulation study. *Virology.* 233:163–173.
35. Torres, J., A. Kukol, and I. T. Arkin. 2000. Use of a single glycine residue to determine the tilt and orientation of a transmembrane helix. A new structural label for infrared spectroscopy. *Biophys. J.* 79:3139–3143.

36. Wang, J., S. Kim, F. Kovacs, and T. A. Cross. 2001. Structure of the transmembrane region of the M_2 protein H^+ channel. *Protein Sci.* 10: 2241–2250.

37. Kovacs, F. A., and T. A. Cross. 1997. Transmembrane four-helix bundle of influenza A M_2 protein channel: structural implications from helix tilt and orientation. *Biophys. J.* 73:2511–2517.

38. Nishimura, K., S. Kim, L. Zhang, and T. A. Cross. 2002. The closed state of a H^+ channel helical bundle combining precise orientational and distance restraints from solid state NMR. *Biochemistry.* 41:13170–13177.

39. Duong-Ly, K. C., V. Nanda, W. F. Degrado, and K. P. Howard. 2005. The conformation of the pore region of the M_2 proton channel depends on lipid bilayer environment. *Protein Sci.* 14:856–861.

40. Gandhi, C. S., K. Shuck, J. D. Lear, G. R. Dieckmann, W. F. DeGrado, R. A. Lamb, and L. H. Pinto. 1999. Cu(II) inhibition of the proton translocation machinery of the influenza A virus M_2 protein. *J. Biol. Chem.* 274:5474–5482.

41. Wu, C. H., A. Ramamoorthy, and S. J. Opella. 1994. High-resolution heteronuclear dipolar solid-state NMR spectroscopy. *J. Mag. Res. A.* 109:270–272.

42. Ramamoorthy, A., Y. Wei, and D. K. Lee. 2004. PISEMA solid-state NMR spectroscopy. *Ann. Rep. NMR Spectrosc.* 52:1–52.

43. Barlos, K., D. Papaioannou, and D. Theodoropoulos. 1982. Efficient one-pot synthesis of *n*-trityl amino acids. *J. Org. Chem.* 47:1324–1326.

44. Chang, C. D., M. Waki, M. Ahmad, J. Meienhofer, E. O. Lundell, and J. D. Haug. 1980. Preparation and properties of Nα-9-fluorenylmethyloxycarbonylamino acids bearing tert.-butyl side chain protection. *Int. J. Pept. Protein Res.* 15:59–66.

45. Sanders, C. R., and K. Oxenoid. 2000. Customizing model membranes and samples for NMR spectroscopic studies of complex membrane proteins. *Biochim. Biophys. Acta.* 1508:129–145.

46. Mimms, L. T., G. Zampighi, Y. Nozaki, C. Tanford, and J. A. Reynolds. 1981. Phospholipid vesicle formation and transmembrane protein incorporation using octyl glucoside. *Biochemistry.* 20:833–840.

47. Koynova, R., and M. Caffrey. 1998. Phases and phase transitions of the phosphatidylcholines. *Biochim. Biophys. Acta.* 1376:91–145.

48. Yamamoto, K., D. K. Lee, and A. Ramamoorthy. 2005. Broadband-PISEMA solid-state NMR spectroscopy. *Chem. Phys. Lett.* 407:289–293.

49. Yamamoto, K., S. V. Dvinskikh, and A. Ramamoorthy. 2006. Measurement of heteronuclear dipolar couplings using a rotating frame solid-state NMR experiment. *Chem. Phys. Lett.* 419:533–536.

50. Fu, R., J. Hu, and T. A. Cross. 2004. Towards quantitative measurements in solid-state CPMAS NMR: a Lee-Goldburg frequency modulated cross-polarization scheme. *J. Magn. Reson.* 168:8–17.

51. Blasco, T., J. Perez-Pariente, and W. Kolodziejski. 1997. A solid-state NMR study of the molecular sieve VPI-5 synthesized in the presence of a CTABr surfactant. *Solid State Nucl. Magn. Reson.* 8:185–194.

52. Hu, J., R. Fu, K. Nishimura, L. Zhang, H. X. Zhou, D. D. Busath, V. Vijayvergiya, and T. A. Cross. 2006. Histidines, heart of the hydrogen ion channel from influenza A virus: toward an understanding of conductance and proton selectivity. *Proc. Natl. Acad. Sci. USA.* 103:6865–6870.

53. Blomberg, F., W. Maurer, and H. Ruterjans. 1977. Nuclear magnetic resonance investigation of 15N-labeled histidine in aqueous solution. *J. Am. Chem. Soc.* 99:8149–8159.

54. Hu, J. 2005. Structure-function correlation of the M_2 proton channel characterized by solid-state nuclear magnetic resonance spectroscopy. PhD thesis. Florida State University, Tallahassee, FL.

55. Tian, F., and T. A. Cross. 1997. Dipolar oscillations in cross-polarized peptide samples in oriented lipid bilayers. *J. Magn. Reson.* 125:220–223.

56. Kolodziejski, W., and J. Klinowski. 2002. Kinetics of cross-polarization in solid-state NMR: a guide for chemists. *Chem. Rev.* 102:613–628.

57. Ernst, R. R., G. Bodenhausen, and A. Wokaun. 1987. Principles of Nuclear Magnetic Resonance in One and Two Dimensions. Oxford University Press, Oxford.

58. Demco, D. E., J. Tegenfeldt, and J. S. Waugh. 1975. Dynamics of cross relaxation in nuclear magnetic double-resonance. *Phys. Rev.* 11:4133–4151.

59. Alemany, L. B., D. M. Grant, T. D. Alger, and R. J. Pugmire. 1983. Cross-polarization and magic angle sample spinning NMR-spectra of model organic compounds. 3. Effect of the C-13-H-1 dipolar interaction on cross-polarization and carbon-proton dephasing. *J. Am. Chem. Soc.* 105:6697–6704.

60. Reynolds, W. F., I. R. Peat, M. H. Freedman, and J. R. Lyerla. 1973. Determination of tautomeric form of imidazole ring of L-histidine in basic solution by C-13 magnetic-resonance spectroscopy. *J. Am. Chem. Soc.* 95:328–331.

61. Song, X. J., and A. E. McDermott. 2001. Proton transfer dynamics and N-H bond lengthening in N-H···N model systems: a solid-state NMR study. *Magn. Reson. Chem.* 39:S37–S43.

62. Lunin, V. V., E. Dobrovetsky, G. Khutoreskaya, R. Zhang, A. Joachimiak, D. A. Doyle, A. Bochkarev, M. E. Maguire, A. M. Edwards, and C. M. Koth. 2006. Crystal structure of the CorA Mg^{2+} transporter. *Nature.* 440:833–837.